The influence of hydrostatic pressure and annealing conditions on the magnetostructural transitions in MnCoGe

Jing-Han Chen,[1,a)] Tej Poudel Chhetri,[1] Chung-Kai Chang,[2] Yu-Ching Huang,[3] David P. Young,[1] Igor Dubenko,[4] Saikat Talapatra,[4] Naushad Ali,[4] and Shane Stadler[1]

AFFILIATIONS

[1]Department of Physics and Astronomy, Louisiana State University, Baton Rouge, Louisiana 70803, USA
[2]National Synchrotron Radiation Research Center, Hsinchu 30076, Taiwan
[3]Department of Materials Engineering, Ming Chi University of Technology, New Taipei City 24301, Taiwan
[4]Department of Physics, Southern Illinois University, Carbondale, Illinois 62901, USA

[a)]**Author to whom correspondence should be addressed:** jhchen10@lsu.edu

ABSTRACT

In this work, the phase transitions of stoichiometric MnCoGe alloys were studied by systematically varying the annealing conditions and applying hydrostatic pressure. First-order martensitic structural transitions from the Ni_2In-type hexagonal austenite phase to the TiNiSi-type orthorhombic martensite phase spanned a wide temperature window (>200 K) as a result of quenching the samples at temperatures ranging from the solid phase at 700 °C to the liquid phase at 1150 °C. Despite the large variation in their structural transition temperatures, the changes in cell parameters across the structural transitions and the Curie–Weiss temperatures of the martensite/austenite phase were relatively small. For the sample quenched from 800 °C, coupled magnetostructural transitions were observed, and the largest maximum magnetic entropy change was found to be $-\Delta S_{max} = 33.6$ J/kg K for a 7-T field change. The coupled magnetostructural transitions and the corresponding magnetic entropy enhancements were found to also be achievable by applying hydrostatic pressures. Meanwhile, as the quenching temperatures or hydrostatic pressures increased, the first-order martensitic structural transition shifted toward lower temperature until it was ultimately absent, in which case only the crystal structure and magnetic transition of the Ni_2In-type hexagonal austenite phase were present.

I. INTRODUCTION

Studies of magnetostructural phase transitions in magnetic materials have intensified due to the potential energy-saving and climate-friendly advantages of solid state cooling resulting from the magnetocaloric effect (MCE).[1–6] An increasing effort has been put on understanding the physical origins of these effects, as well as discovering better magnetocaloric materials.[7–9] Until now, many solid materials have been studied for scientific and practical purposes with regard to their magnetocaloric properties, including $Gd_5Si_xGe_{4-x}$,[10,11] Ni-Mn-based full Heusler alloys,[12–18] MnAs-based compounds,[19–21] Fe_2P-based alloys,[21–23] $LaFe_{13-x}Si_x$ related compounds,[24,25] and intermetallic Mn*TX* (*T* = transition metal and *X* = Ge, Si) systems.[26–32]

Among the materials listed above, intermetallic Mn*TX* systems have drawn increasing attention recently due to their giant magnetocaloric and baroclaoric effects caused by their large volume expansion/contraction resulting from first-order martensitic structural transitions between a Ni_2In-type hexagonal austenite phase (space group: $P6_3/mmc$) and a TiNiSi-type orthorhombic martensite phase (space group: *Pnma*).[30,31] The MnCoGe-based systems have drawn considerable interest since the structural phase transition (470 K) and Curie temperature (345 K) of the parent MnCoGe compound are relatively close to room temperature.[33] An interesting feature of MnCoGe-based alloys is the strong interplay between their structural and magnetic phase transitions. Several factors, such as the partial substitution with a fourth element,[34–56] stoichiometry modification,[57–59] interstitial doping,[60] vacancy tuning,[61–63] heat treating,[64–66] and pressure application[67] were found to influence the structural and magnetic properties considerably.

In this work, stoichiometric MnCoGe compounds were prepared by annealing the samples at temperatures ranging from 700 °C (solid phase) to 1150 °C (liquid phase), followed by either slowly cooling or rapidly quenching, and the phase transition properties in response to temperature, hydrostatic pressure, and magnetic field were measured. First, the raise of the quenching temperatures was found to lower the first-order martensitic structural transition by over 200 K. The lowest first-order martensitic structural transition temperature (234 K) was observed for the sample quenched at 1000 °C, and the highest one (470 K) was observed for the samples cooled slowly from 1100 °C at 30 °C/h. The largest maximum magnetic entropy change (−33.6 J/kg K for a 7-T field change) was found for the samples quenched at 800 °C, for which the magnetic and structural phase transitions are coupled. Second, as we increased the hydrostatic pressure, the first-order martensitic structural transition shifted to lower temperature until the samples were completely converted to the Ni_2In-type hexagonal austenite phase with second-order magnetic phase transitions. Our findings show that the first-order martensitic structural transition was suppressed and transformed to a second-order magnetic phase transition of the Ni_2In-type hexagonal austenite phase when either quenched from sufficiently high temperatures or subjected to sufficiently high hydrostatic pressures.

II. THERMAL ANALYSIS

The formation of the MnCoGe compounds was explored using a simultaneous differential scanning calorimeter (DSC) and thermogravimetric analysis device (model: SDT Q600 manufactured by TA Instruments, Inc.). To explore the synthesis of MnCoGe alloys, the individual pure elements were placed in the DSC, and the heat flow measurement was carried out by sweeping the temperature up to 1100 °C twice as shown in Fig. 1. The first heating experimental route is shown in Fig. 1(a), and the allotropic transformation of Mn was observed at 720 °C,[68] followed by the complete liquification of MnCoGe components at 1100 °C. A clear first-order phase transition peak due to crystallization was observed at 1050 °C in the first cooling route.

After the samples were cooled, second heating and cooling scans were performed. In the second cycle, the melting/crystallization of the MnCoGe ingot was observed as shown in Fig. 1(b), and no other perceivable transitions were observed. Guided by these results, a MnCoGe ingot was prepared by melting it at 1100 °C, and was then quenched either in the solid or liquid phase at the selected temperatures described in Sec. III.

In addition to exploring the potential synthesis conditions, DSC experiments were also performed for the samples with nonmagnetic first-order martensitic structural transitions occurring above 400 K, the results of which together with those of magnetization measurements, will be discussed in Sec. V.

III. SAMPLE PREPARATION

In order to fabricate stoichiometric MnCoGe, high purity Mn (99.95%), Co (99.95%), and Ge (99.999%) elemental components were placed inside Al_2O_3 crucibles, and then sealed in a quartz tube under vacuum. The materials were then brought up to 1100 °C and annealed for 12 h. To ensure the homogeneity of their chemical

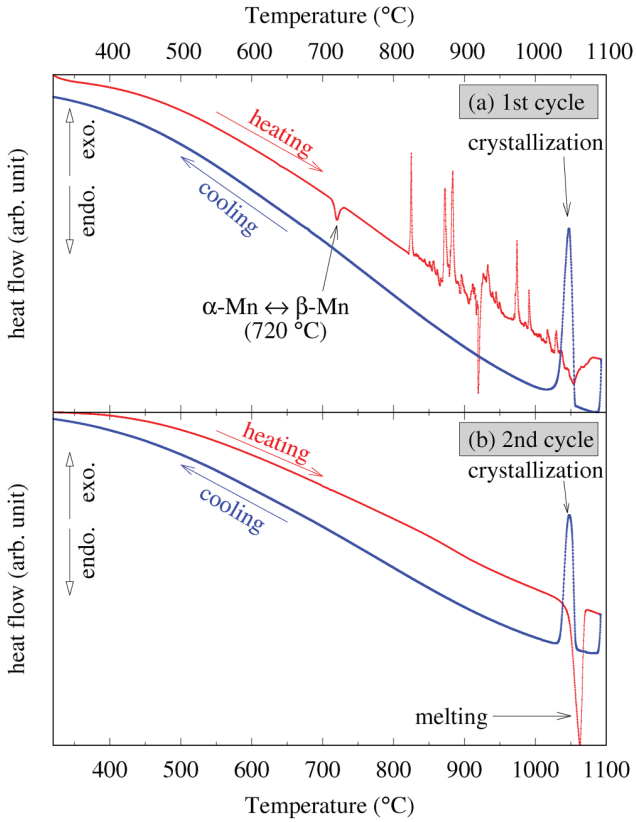

FIG. 1. The heat flow curves of stoichiometric MnCoGe formed from the pure constituent elements during (a) 1st cycle and (b) 2nd cycle of the DSC experiments. In the 1st heating scan, the allotropic transformation of Mn was observed at 720 °C followed by the formation of liquid MnCoGe at 1100 °C. In the 2nd heating and cooling scans, first-order phase transitions with thermal hysteresis due to the melting/crystallization of the MnCoGe ingot between 1020 and 1070 °C are the only perceivable transitions.

compositions, the ingots were pulverized and annealed at 1100 °C for another 12 h, and finally cooled to room temperature at 30 °C/h. This 30-g sample served as the source ingot for later sample preparation and is labeled as SC1100, where "SC" stands for "slowly cooled."

Subsequently, 2-g pieces from the source sample were weighed and then melted in an arc furnace to preserve a single and contiguous specimen. Again, they were placed in Al_2O_3 crucibles and then sealed in a quartz tube under vacuum. Since all of the samples in this work were fabricated from the same master ingot, their compositions were expected to be identical. The samples were annealed separately at 1150, 1000, 900, 800, and 700 °C for 12 h (labeled as AQ1150, AQ1000, AQ900, AQ800, and AQ700, respectively), and then quenched in a vessel of liquid nitrogen by breaking the quartz tube. Note that sample AQ1150 was quenched from the liquid phase, while the others remained solidified during annealing. The synthesis conditions of all the samples and their respective properties are summarized in Table I.

TABLE I. The annealing conditions of the samples and their corresponding properties.

Label	Annealing condition (°C)		Martensite[a] $\theta_{CW}(K)$	T_m[b] (K)	Austenite[a] θ_{CW} (K)	$-\Delta S_{max}$[c] (J/kg K)	δ_{FWHM}[d] (K)	RCP[e] (J/kg)	M_{sat}/f.u. (μ_B)
SC1100	1100	(slowly cooled)	353	470	—	—	—	—	3.87
AQ700	700	(solid quenched)	355	417	—	—	—	—	3.79
AQ800	800	(solid quenched)	—	333	317	33.6	12	403	3.79
AQ900	900	(solid quenched)	—	270	304	9.7	57	553	3.86
AQ1000	1000	(solid quenched)	—	234	295	9.6	71	682	3.79
AQ1150	1150	(liquid quenched)	—	—	278	—	—	—	2.72

[a]θ_{CW} is the Curie–Weiss temperature of the martensite or austenite phase, estimated by fitting with the Curie–Weiss law as described in Sec. V C.
[b]T_m is the first-order martensitic structural transition temperature, estimated from the magnetization and calorimetric results shown in Fig. 5.
[c]ΔS_{max} estimated from isothermal magnetization measurements described in Sec. V D.
[d]δ_{FWHM} full width at half maximum of the entropy change $\Delta S(T)$.
[e]RCP, the relative cooling power, was estimated using $RCP = \Delta S_{max} \times \delta_{FWHM}$ for $\mu_0 \Delta H = 7$ T.[69,70]

IV. X-RAY DIFFRACTION

The crystal structures of the samples were investigated by powder x-ray diffraction (XRD), which was performed using a Scintag XDS2000 powder diffractometer with Cu Kα radiation at room temperature. To avoid the induced stress/stain due to the grinding process,[71,72] the XRD samples were prepared by thermal cycling the samples back and forth across their structural transitions until they were broke down into powders. The XRD results at room-temperature for all samples are shown in Fig. 2.

According to the XRD results, samples SC1000, AQ700, and AQ800 crystallized in the TiNiSi-type orthorhombic martensite phase at room temperature, while samples AQ900, AQ1000, and AQ1150 crystallized in the Ni_2In-type hexagonal austenite phase. The lattice parameters and cell volumes of their major crystal structures are tabulated in Table II, which were obtained from Rietveld refinements using general structure analysis system (GSAS) software.[73–76] As the annealing temperature increased, the cell volumes per MnCoGe formula unit at room temperature decreased. As the volume reduces, the first-order martensitic structural transition temperatures also reduce, which has been commonly observed in similar materials,[77,78] because the Ni_2In-type hexagonal austenite phase has a smaller volume than that of the TiNiSi-type orthorhombic martensite phase.

It is known that the TiNiSi-type orthorhombic martensite phase can be regarded as a distortion of the Ni_2In-type hexagonal austenite phase through the relations $a_{orth} \leftrightarrow c_{hex}$, $b_{orth} \leftrightarrow a_{hex}$, and $c_{orth} \leftrightarrow \sqrt{3}a_{hex}$.[27] Based on these relations, the distortion relations between the annealing temperatures and crystal parameters/volume are presented in Fig. 3. As the annealing temperature increases, a 10.6% reduction of a_{orth} and a 6.9% expansion of b_{orth} were observed, resulting in a 3.9% volume reduction overall. Note that the deformations of the cell parameters $a_{orth} \leftrightarrow c_{hex}$ and $b_{orth} \leftrightarrow a_{hex}$ are relatively larger than that of $c_{orth} \leftrightarrow \sqrt{3}a_{hex}$, which is commonly observed in alloys with a structural transformation from a Ni_2In-type hexagonal austenite phase to a TiNiSi-type orthorhombic martensite phase.[77,78]

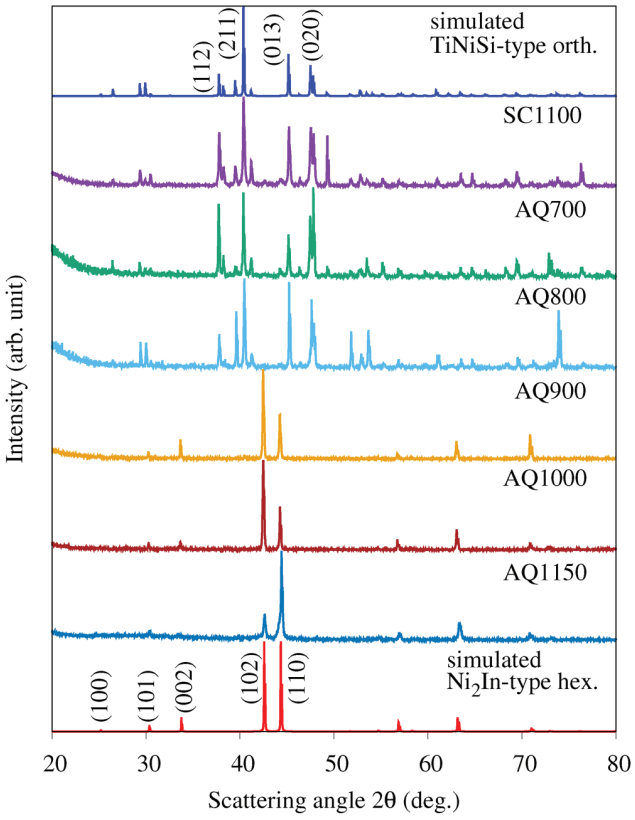

FIG. 2. Powder x-ray diffraction results at room temperature. For comparison, the pattern in the top panel shows the results of the ideal TiNiSi-type orthorhombic structure, and the pattern in the bottom panel shows the results of the ideal Ni_2In-type MnCoGe hexagonal structure. As the annealing temperature increases, the fraction of the Ni_2In-type hexagonal austenite phase increases at the expense of the TiNiSi-type orthorhombic structure.

TABLE II. The lattice parameters and cell volumes calculated from room temperature powder diffraction data.

Label	Major phase	a(Å)	b(Å)	c(Å)	vol./f.u.(Å^3)
SC1100	TiNiSi	5.966	3.822	7.059	40.23
AQ700	TiNiSi	5.952	3.822	7.053	40.11
AQ800	TiNiSi	5.946	3.825	7.052	40.10
AQ900	Ni_2In	4.090	4.090	5.317	38.52
AQ1000	Ni_2In	4.084	4.084	5.312	38.37
AQ1150	Ni_2In	4.075	4.075	5.300	38.11

To investigate the structural changes across the martensitic structural transitions, samples AQ900 and SC1100 were selected for temperature-dependent XRD experiments, which were performed at the X-ray Science Division beamlines at the Advanced Photon Source, Argonne National Laboratory and the National Synchrotron Radiation Research Center (NSRRC, Taiwan) on beamline TLS-01C2, respectively. These temperature dependent XRD results are shown in Fig. 4. As the temperature increases through the martensitic structural transitions, the TiNiSi-type orthorhombic martensite phase at low temperature distorts with a

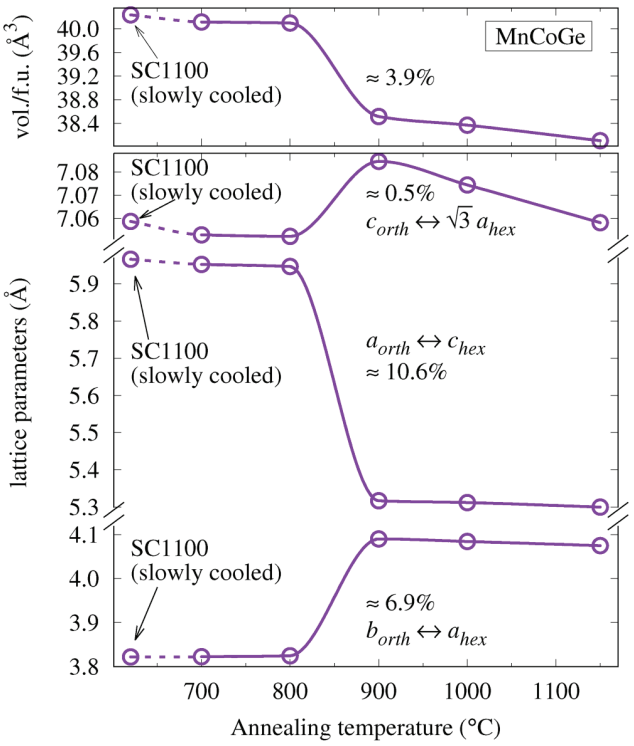

FIG. 3. Lattice parameters and cell volumes per MnCoGe formula unit at room temperature vs the annealing temperatures are shown along with the corresponding distortion percentages. The cell volumes decrease as the annealing temperature increases. A relatively large distortion due to a reduced a_{orth} and an expanded b_{orth} was observed, while c_{orth} remains relatively unchanged.

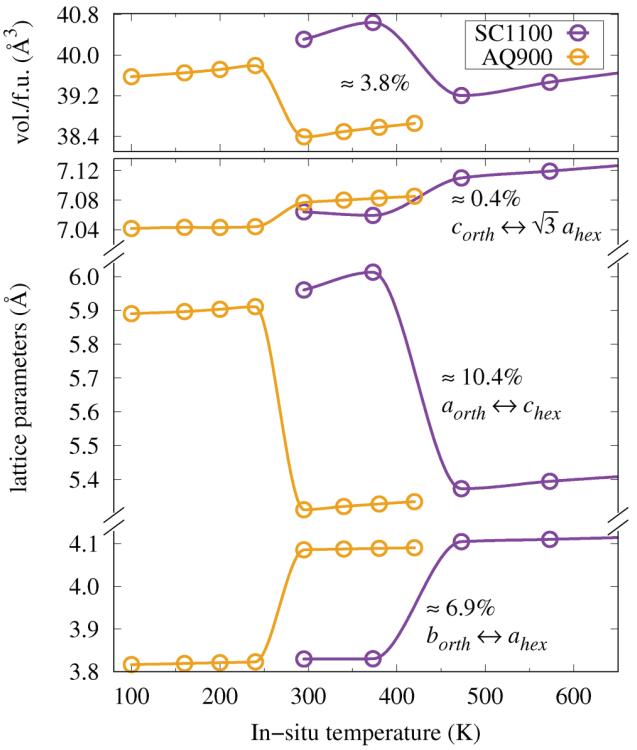

FIG. 4. Cell volumes/parameters for samples SC1100 and AQ900 acquired from temperature-dependent XRD. The changes in cell volumes/parameters across the martensitic structural transitions for these three samples are nearly the same, although a coupled magnetostructural transition was observed only in sample AQ900, not sample SC1100.

10.4% reduction of a_{orth} and 6.9% expansion of b_{orth}, and ultimately stabilizes in the Ni_2In-type hexagonal austenite phase. The changes in cell parameters across the martensitic structural transitions for these samples are nearly the same although their transition temperatures are significantly separated, and a coupled magnetostructural transition was observed only in sample AQ900, not sample SC1100. Comparable magnitude changes of the cell parameters were reported previously by sweeping across the first-order martensitic structural transition temperatures of MnCoGe[27] or $MnCoGe_{1-x}In_x$ ($x = 0.01, 0.02$),[79] or by substituting Cu in $Mn_{1-x}Cu_xCoGe$.[42]

V. MAGNETIZATION MEASUREMENTS AND ANALYSIS

The magnetization results presented in this section were obtained using a magnetic property measurement system manufactured by Quantum Design, in a temperature range of 20–400 K and in fields up to 7 T.

A. Temperature-dependent magnetization

The isofield, temperature-dependent magnetization measurements in an applied 0.1-T field were performed using field-cooled

cooling and field-cooled warming protocols, and the results are shown in Fig. 5. At ambient pressure, all the samples except AQ1150 exhibit first-order martensitic structural transitions with thermal hysteresis. First-order martensitic structural transitions were not observed in sample AQ1150, which is consistent with the MnCoGe samples prepared by melt spinning,[66] while the sample SC1100 shows similar structural and magnetic transitions as reported in Ref. 33.

The first-order martensitic structural transition temperatures, T_m, estimated from the temperature-dependent magnetization measurements and the calorimetric experiments, are listed in Table I. Increasing annealing temperatures were found to decrease the first-order martensitic structural transition temperatures rapidly, and to decrease the Curie–Weiss temperature of austenite phase comparatively slowly. The lowest first-order martensitic structural transition temperature (234 K) was observed for the sample quenched at 1000 °C, and the highest one (470 K) was observed for the sample cooled slowly from 1100 °C. The effect of the annealing temperatures on the first-order martensitic structural transitions and Curie–Weiss temperatures is illustrated in Fig. 6.

Magnetization measurements under hydrostatic pressure were performed using a commercial BeCu cylindrical pressure cell manufactured by HMD Inc.[80,81] The temperature-dependent magnetization results in 0.1-T field shown in Fig. 5 (dashed lines) demonstrate the effect of pressure on the phase transitions under the indicated hydrostatic pressures. With the specified hydrostatic pressures, the thermal hysteresis due to the first-order martensitic structural transitions was suppressed in samples AQ900 (8.9 kbar) and AQ1000 (8.3 kbar), while the first-order martensitic structural transition temperatures decreased in samples SC1100 (11.3 kbar) and AQ700 (6.4 kbar). These temperature-dependent magnetization results under pressures suggest that the hydrostatic pressure application induces the negative temperature shift of martensitic structural transitions, and the absence of the first-order martensitic structural transition was observed as long as sufficiently high pressure is applied. Note that the first-order martensitic structural transition was expected to convert to second-order phase transition in samples SC1100, AQ700, and AQ800 if sufficiently high pressures were applied. In summary, it is found that the first-order

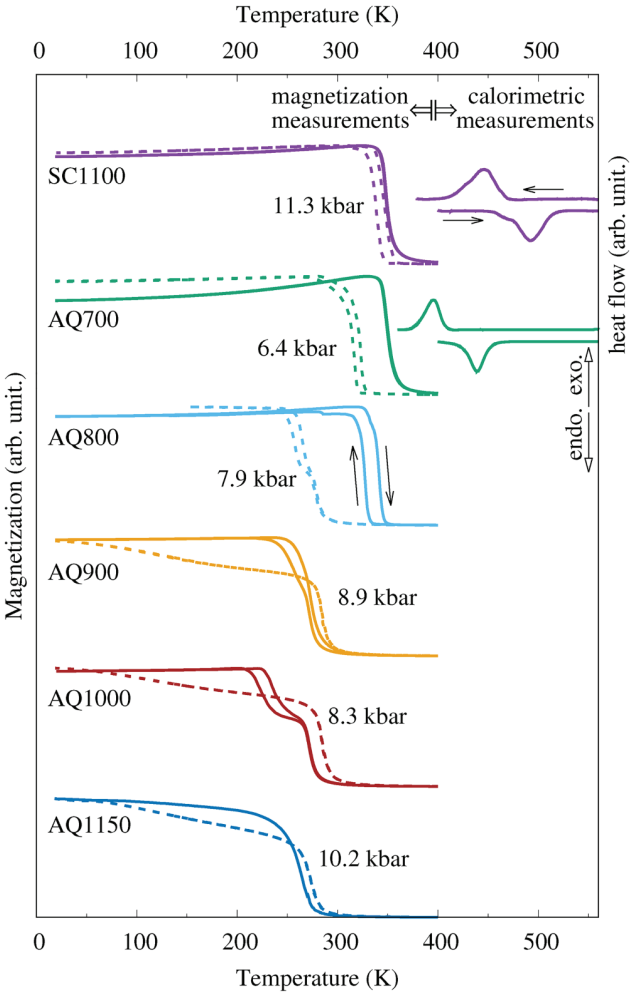

FIG. 5. The temperature-dependent magnetization of all samples (solid lines represent the results measured at ambient pressure, whereas dashed lines represent those measured at the indicated pressures) using field-cooled cooling and field-cooled warming protocols at $H = 0.1$ T. For samples SC1100 and AQ700 with first-order martensitic structural transitions above 400 K, calorimetric experiments are shown in the upper right side of this figure. The temperature sweeping directions are indicated by arrows in the magnetization data of sample AQ800 and calorimetric results of sample SC1100. The first-order martensitic structural transition temperatures converted to second-order magnetic phase transitions in the Ni_2In-type hexagonal austenite phase when the applied pressures or annealing temperatures were sufficiently high.

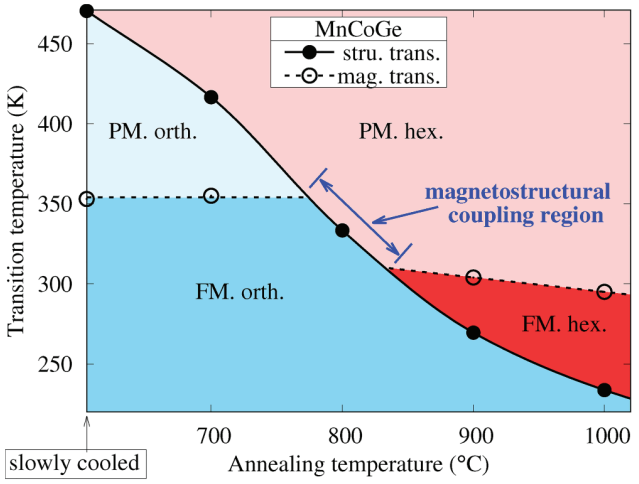

FIG. 6. A phase diagram illustrating the effect of annealing temperatures on the first-order martensitic structural transition temperatures (solid lines) and Curie–Weiss temperatures (dashed lines).

martensitic structural transitions were converted to second-order magnetic phase transitions of the Ni_2In-type hexagonal austenite phase by either applying pressures or raising the quenching temperatures.

B. Field-dependent magnetization

To further investigate the magnetizations of the samples at low temperatures, saturation magnetization measurements at 2.0 K were performed up to 7 T, as shown in Fig. 7. The saturation magnetization (M_{sat}) values were estimated by fitting the experimental magnetization data by the law of approach-to-saturation

$$M(H) = M_{sat}\left(1 - \frac{a}{H^2} - \frac{b}{H^3}\right),$$

where a and b are fitting parameters.[82,83] These fitted M_{sat} values are listed in Table I. Different from the other quenched samples, sample AQ1150 shows a much lower saturation magnetization and also exhibits no thermal hysteresis in the temperature-dependent magnetization, as shown in Fig. 5. With the application of hydrostatic pressures, similar phenomena were observed in samples AQ900 (8.9 kbar) and AQ1000 (8.3 kbar). It is known that the saturation magnetization of the MnCoGe parent phase is 3.9 and 2.6 μ_B for the TiNiSi-type orthorhombic martensite phase and the Ni_2In-type hexagonal austenite phase, respectively.[27,84–87] Therefore, the abrupt reduction of the saturation magnetization along with the absence of thermal hysteresis observed here are concluded to be evidence that the TiNiSi-type orthorhombic martensite phase was completely suppressed, and only the Ni_2In-type hexagonal austenite phase was present under the specified annealing and pressure conditions.

C. Curie–Weiss law analysis

The Curie–Weiss law[88]

$$\frac{1}{\chi} = \frac{H}{M} = (T - \theta_{CW})\frac{3k_B}{N_A\mu_{eff}^2},$$

where N_A is Avogadro's number, k_B is the Boltzmann constant, μ_{eff} is the effective magnetic moments per formula unit, and θ_{CW} is the Curie–Weiss temperature, was used to fit the temperature-dependent magnetization in the paramagnetic temperature region. The linearity between $1/\chi$ and T shown in Fig. 8 demonstrates the paramagnetic behavior of both the martensite and austenite phases. The fitted Curie–Weiss temperatures for the Ni_2In-type austenite phase and for the TiNiSi-type orthorhombic martensite phase are listed in Table I, and these values are consistent with previous reports.[67,85,87] It is worth noting that the Curie–Weiss temperatures of both the TiNiSi-type orthorhombic martensite phase and the Ni_2In-type austenite phase remain relatively unchanged regardless of the annealing and pressure conditions, while the first-order martensitic structural transition temperatures are sensitive to both.

D. Magnetic entropy change

The potential MCE performance of materials was characterized by the magnetic entropy change $\Delta S(T, 0 \rightarrow H)$, which was

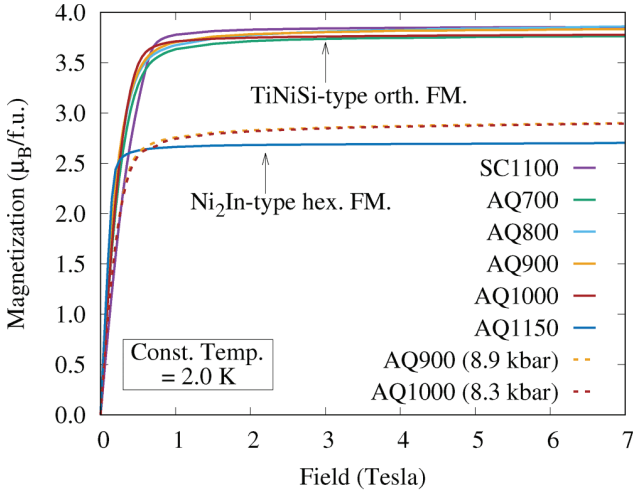

FIG. 7. The isothermal magnetization curves at 2.0 K at ambient and specified pressures were performed in fields up to 7 T. The abrupt decrease in the saturation magnetization for samples AQ1150, AQ900 (8.9 kbar), and AQ1000 (8.3 kbar) are evidence that the TiNiSi-type orthorhombic martensite phase was absent and only the Ni_2In-type hexagonal austenite phase was present under their specified annealing and pressure conditions.

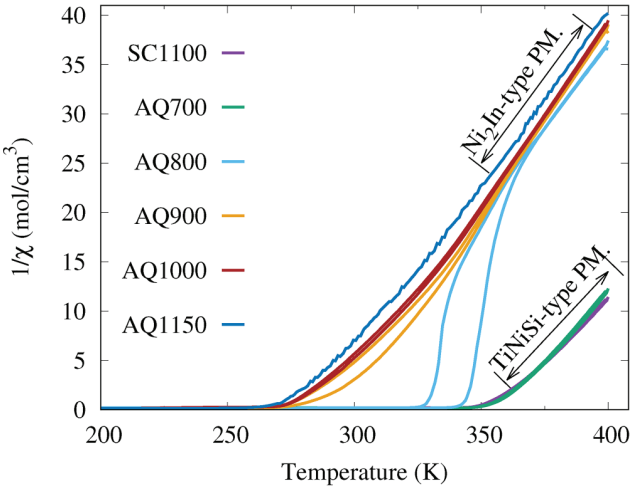

FIG. 8. Curie–Weiss plots, i.e., $1/\chi$ vs temperature, constructed from the temperature-dependent magnetization results at $H = 0.1$ T. Note that the Curie–Weiss temperatures of both the TiNiSi-type orthorhombic martensite phase and the Ni_2In-type austenite phase remain relatively unchanged regardless of the annealing temperatures or hydrostatic pressure, while the first-order martensitic structural transition temperatures are sensitive to both.

estimated by using the thermodynamic relation[89]

$$\Delta S(T, 0 \rightarrow H) = \frac{\partial}{\partial T}\left(\int_0^H M(T, H')\, dH'\right)_{T=const.} \cong \frac{1}{\Delta T}\left[\int_0^H M(T + \Delta T, H')\, dH' - \int_0^H M(T, H')\, dH'\right].$$

A series of isothermal magnetization measurements were performed to obtain $M(T = const., H)$. To eliminate any residual ferromagnetic response from the martensite phase, prior to each isothermal magnetization measurement the samples were heated to complete the paramagnetic austenite phase, and then cooled down to the target measurement temperature under zero field. This thermodynamic reset protocol was referred to as the cooling protocol or the loop process in Refs. 90 and 91, because the results obtained using this protocol can also be acquired by calorimetric experiments during the cooling process.

The magnetic entropy changes of samples under different quenching temperatures for a 7-T field are shown in Fig. 9. The values of the maximum magnetic entropy change and relative cooling power for each sample are listed in Table I. Sample AQ800 shows the largest maximum magnetic entropy change for a 7-T field change ($\Delta S_{max} = -33.6$ J/kg K) while the other samples have nearly equivalent magnitudes with $\Delta S_{max} = -9.7$ J/kg K for AQ900, and -9.6 J/kg K for AQ1000. Among all the samples, AQ1000 shows the largest relative cooling power ($RCP = 682$ J/kg for a 7-T field change) although its full width at half maximum, δ_{FWHM}, is much larger than that of AQ800. Comparable maximum magnetic entropy changes and martensitic structural transition temperature shifts were also observed in Ref. 59 by controlling the valence electron concentration of $Mn_{1-x}CoGe_{1+x}/Mn_{1+y}CoGe_{1-y}$, and in Ref. 34 by controlling the Au-doping concentration in $Mn_{1-x}Au_xCoGe$. Nevertheless, the results presented here were achieved for samples with a single composition, MnCoGe.

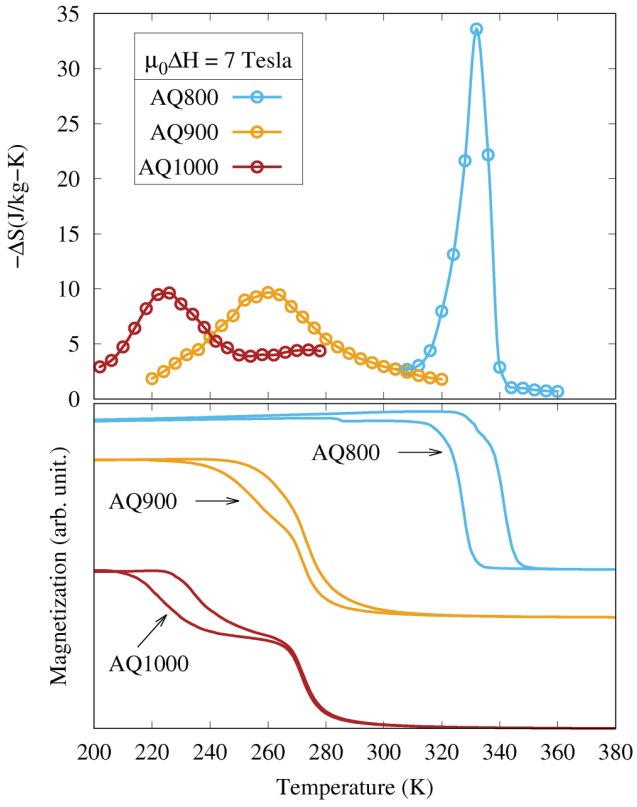

FIG. 9. The magnetic entropy changes (upper figure) for a 7-T field change estimated from magnetization isotherm measurements and the temperature-dependent magnetization (lower figure) using field-cooled cooling and field-cooled warming protocols at 0.1 T of samples AQ800, AQ900, and AQ1000 are shown.

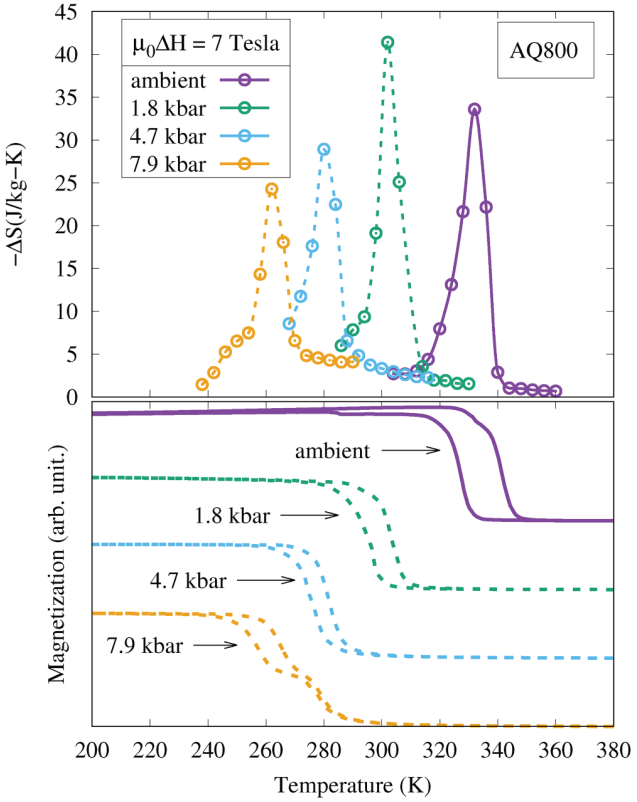

FIG. 10. The magnetic entropy changes (upper figure) for a 7-T field change estimated from magnetization isotherm measurements and the temperature-dependent magnetization (lower figure) using field-cooled cooling and field-cooled warming protocols (solid lines are measured at ambient pressure, whereas dashed lines are measured at the various indicated applied pressures) at 0.1 T of sample AQ800 are shown.

The sample AQ800 that shows the largest maximum magnetic entropy change was selected for further investigation of the magnetic entropy changes under different pressures, the results of which are shown in Fig. 10. Similar to the effect of quenching temperature, hydrostatic pressure drives the martensitic structural transition temperature lower as the pressure increases, and the magnetostructural transitions decoupled. Meanwhile, the maximum magnetic entropy change at 1.8 kbar was found to be largest, and then tended to decrease as the pressure further increased up to 7.9 kbar. It is clear that the pressure induces the negative temperature shift of the martensitic structural transition and would ultimately suppress the first-order martensitic structural transition as long as sufficiently high pressure were applied. Therefore, the maximum magnetic entropy change is expected to be further reduced above 7.9 kbar until the first-order martensitic structural transition is completely absent and only the second-order magnetic transition is present in sufficiently high pressures.

VI. CONCLUSIONS

In this work, the structural and magnetic properties of MnCoGe upon systematic variation of the annealing/quenching conditions and applied hydrostatic pressure were investigated. First-order martensitic structural transitions from the TiNiSi-type orthorhombic martensite phase to the Ni_2In-type hexagonal austenite phase decreased in a wide temperature range (>200 K) by increasing the quenching temperatures of the samples in the solid phase up to 1000 °C. As the samples were quenched from the liquid phase (1150 °C), the first-order martensitic structural transition disappeared, and only the second-order magnetic transition remained. Similarly, as we applied hydrostatic pressures, all of the samples converted to the Ni_2In-type hexagonal austenite phase with a second-order magnetic transition for sufficiently high pressures. It is concluded that the TiNiSi-type orthorhombic martensite phase would eventually be absent, and only the second-order magnetic phase transitions of the Ni_2In-type hexagonal austenite phase would be present, if sufficiently high annealing temperatures or hydrostatic pressures were reached. Meanwhile, the coupled magnetostructural transitions and the corresponding magnetic entropy enhancements were found to also be achievable by either applying proper hydrostatic pressures, quenching conditions, or both.

ACKNOWLEDGMENTS

S. Stadler acknowledges support from the U.S. Department of Energy (DOE), Office of Basic Energy Sciences under Award No. DE-FG02-13ER46946. N. Ali and I. Dubenko acknowledge support from the U.S. Department of Energy, Office of Basic Energy Sciences under Award No. DE-FG02-06ER46291. D. P. Young acknowledges support from the U.S. National Science Foundation (NSF), Division of Materials Research under Award No. NSF-DMR-1904636. Y.-C. Huang acknowledges support from the Ministry of Science and Technology of Taiwan (No. MOST 107-2218-E-131-007-MY3). This research used resources of the Advanced Photon Source, a U.S. Department of Energy (DOE) Office of Science User Facility operated for the DOE Office of Science by the Argonne National Laboratory under Contract No. DE-AC02-06CH11357. The DSC data used in this work were collected at the Center for Advanced Microstructures and Devices (CAMD) under the supervision of A. Roy.

DATA AVAILABILITY

The data that support the findings of this study are available from the corresponding author upon reasonable request.

REFERENCES

[1]E. Brück, O. Tegus, D. C. Thanh, N. T. Trung, and K. H. J. Buschow, Int. J. Refrig. **31**, 763 (2008).
[2]E. Brück, J. Phys. D **38**, R381 (2005).
[3]B. G. Shen, J. R. Sun, F. X. Hu, H. W. Zhang, and Z. H. Cheng, Adv. Mater. **21**, 4545 (2009).
[4]K. A. Gschneidner and V. K. Pecharsky, Int. J. Refrig. **31**, 945 (2008).
[5]K. A. Gschneidner, Jr., V. K. Pecharsky, and A. O. Tsokol, Rep. Prog. Phys. **68**, 1479 (2005).
[6]V. Franco, J. S. Blázquez, B. Ingale, and A. Conde, Annu. Rev. Mater. Res. **42**, 305 (2012).
[7]K. G. Sandeman, Scr. Mater. **67**, 566 (2012).
[8]C. A. C. Garcia, J. D. Bocarsly, and R. Seshadri, Phys. Rev. Mater. **4**, 024402 (2020).
[9]J. D. Bocarsly, E. E. Levin, C. A. C. Garcia, K. Schwennicke, S. D. Wilson, and R. Seshadri, Chem. Mater. **29**, 1613 (2017).
[10]J. R. Sun, B. G. Shen, and F. X. Hu, in *Nanoscale Magnetic Materials and Applications*, edited by J. Ping Liu, O. Gutfleisch, E. Fullerton, and D. J. Sellmyer (Springer Science+Business Media, 2009), Chap. 15, pp. 472–476.
[11]V. K. Pecharsky and K. A. Gschneidner, Jr., Phys. Rev. Lett. **78**, 4494 (1997).
[12]Y. Sutou, Y. Imano, N. Koeda, T. Omori, R. Kainuma, K. Ishida, and K. Oikawa, Appl. Phys. Lett. **85**, 4358 (2004).
[13]T. Krenke, E. Duman, M. Acet, E. F. Wassermann, X. Moya, L. Mañosa, and A. Planes, Nat. Mater. **4**, 450 (2005).
[14]M. Khan, N. Ali, and S. Stadler, J. Appl. Phys. **101**, 053919 (2007).
[15]F. S. Liu, Q. B. Wang, W. Q. Ao, Y. J. Yu, L. C. Pan, and J. Q. Li, J. Magn. Magn. Mater. **324**, 514 (2012).
[16]L. H. Bennett, V. Provenzano, R. D. Shull, I. Levin, E. D. Torre, and Y. Jin, J. Alloys Compd. **525**, 34 (2012).
[17]T. Krenke, E. Duman, M. Acet, E. F. Wassermann, X. Moya, L. Mañosa, A. Planes, E. Suard, and B. Ouladdiaf, Phys. Rev. B **75**, 104414 (2007).
[18]J.-H. Chen, N. M. Bruno, I. Karaman, Y. Huang, J. Li, and J. H. Ross, Jr., Acta Mater. **105**, 176 (2016).
[19]H. Wada, T. Morikawa, K. Taniguchi, T. Shibata, Y. Yamada, and Y. Akishige, Physica B **328**, 114 (2003).
[20]L. Tocado, E. Palacios, and R. Burriel, J. Therm. Anal. Calorim. **84**, 213 (2006).
[21]O. Tegus, E. Brück, K. H. J. Buschow, and F. R. de Boer, Nature **415**, 150 (2002).
[22]N. T. Trung, Z. Q. Ou, T. J. Gortenmulder, O. Tegus, K. H. J. Buschow, and E. Brück, Appl. Phys. Lett. **94**, 102513 (2009).
[23]N. H. Dung, Z. Q. Ou, L. Caron, L. Zhang, D. T. C. Thanh, G. A. de Wijs, R. A. de Groot, K. H. J. Buschow, and E. Brück, Adv. Energy Mater. **1**, 1215 (2011).
[24]F.-X. Hu, B.-G. Shen, J.-R. Sun, Z.-H. Cheng, G.-H. Rao, and X.-X. Zhang, Appl. Phys. Lett. **78**, 3675 (2001).
[25]L. F. Bao, F. X. Hu, L. Chen, J. Wang, J. R. Sun, and B. G. Shen, Appl. Phys. Lett. **101**, 162406 (2012).
[26]V. Johnson and C. G. Frederick, Phys. Status Solidi A **20**, 331 (1973).
[27]V. Johnson, Inorg. Chem. **14**, 1117 (1975).
[28]K. Morrison, A. Barcza, J. D. Moore, K. G. Sandeman, M. K. Chattopadhyay, S. B. Roy, A. D. Caplin, and L. F. Cohen, J. Phys. D **43**, 195001 (2010).
[29]S. Anzai and K. Ozawa, Phys. Rev. B **18**, 2173 (1978).

[30]W. Bażela, A. Szytuła, J. Todorović, Z. Tomkowicz, and A. Zięba, Phys. Status Solidi A **38**, 721 (1976).
[31]H. Fjellvåg and A. F. Andresen, J. Magn. Magn. Mater. **50**, 291 (1985).
[32]V. K. Sharma, M. A. Manekar, H. Srivastava, and S. B. Roy, J. Phys. D **49**, 50LT01 (2016).
[33]S. Nizioł, A. Wesełucha, W. Bażela, and A. Szytuła, Solid State Commun. **39**, 1081 (1981).
[34]J.-H. Chen, A. Trigg, T. Poudel Chhetri, D. P. Young, I. Dubenko, N. Ali, and S. Stadler, J. Appl. Phys. **127**, 213901 (2020).
[35]Q. Ren, W. D. Hutchison, J. Wang, A. J. Studer, and S. J. Campbell, Chem. Mater. **30**, 1324 (2018).
[36]Y. Wang, V. Yannello, J. Graterol, H. Zhang, Y. Long, and M. Shatruk, Chem. Mater. **32**, 6721 (2020).
[37]X. Si, Y. Liu, X. Ma, J. Lin, J. Yang, and T. Zhou, J. Mater. Sci. **54**, 3196 (2019).
[38]A. Aryal, A. Quetz, S. Pandey, T. Samanta, I. Dubenko, M. Hill, D. Mazumdar, S. Stadler, and N. Ali, J. Alloys Compd. **709**, 142 (2017).
[39]N. T. Trung, V. Biharie, L. Zhang, L. Caron, K. H. J. Buschow, and E. Brück, Appl. Phys. Lett. **96**, 162507 (2010).
[40]J. Torrens-Serra, C. A. Biffi, R. Santamarta, V. Recarte, J. I. Pérez-Landazábal, A. Tuissi, and E. Cesari, Mater. Charact. **93**, 24 (2014).
[41]T. Samanta, I. Dubenko, A. Quetz, S. Stadler, and N. Ali, Appl. Phys. Lett. **101**, 242405 (2012).
[42]S. K. Pal, C. Frommen, S. Kumar, B. C. Hauback, H. Fjellvåg, T. G. Woodcock, K. Nielsch, and G. Helgesen, J. Alloys Compd. **775**, 22 (2019).
[43]Q. Y. Ren, W. D. Hutchison, J. L. Wang, A. J. Studer, M. F. M. Din, S. M. Pérez, J. M. Cadogan, and S. J. Campbell, J. Phys. D **49**, 175003 (2016).
[44]S. Yuce, E. K. Doğan, B. Emre, N. M. Bruno, I. Karaman, and H. Yurtseven, J. Supercond. Novel Magn. **30**, 3587 (2017).
[45]C. L. Zhang, H. F. Shi, E. J. Ye, Y. G. Nie, Z. D. Han, and D. H. Wang, J. Alloys Compd. **639**, 36 (2015).
[46]S. C. Ma, Y. X. Zheng, H. C. Xuan, L. J. Shen, Q. Q. Cao, D. H. Wang, Z. C. Zhong, and Y. W. Du, J. Magn. Magn. Mater. **324**, 135 (2012).
[47]G. Meng, O. Tegus, W. Zhang, L. Song, and J. Huang, J. Alloys Compd. **497**, 14 (2010).
[48]X. Si, Y. Shen, X. Ma, S. Chen, J. Lin, J. Yang, T. Gao, and Y. Liu, Acta Mater. **143**, 306 (2018).
[49]J. Zeng, Z. Wang, Z. Nie, and Y. Wang, Intermetallics **52**, 101 (2014).
[50]K. Ozono, Y. Mitsui, R. Y. Umetsu, M. Hiroi, K. Takahashi, and K. Koyama, AIP Conf. Proc. **1763**, 020003 (2016).
[51]S. Lin, O. Tegus, E. Brück, W. Dagula, T. J. Gortenmulder, and K. H. J. Buschow, IEEE Trans. Magn. **42**, 3776 (2006).
[52]T. Samanta, I. Dubenko, A. Quetz, S. Stadler, and N. Ali, J. Appl. Phys. **113**, 17A922 (2013).
[53]D. Choudhury, T. Suzuki, Y. Tokura, and Y. Taguchi, Sci. Rep. **4**, 7544 (2014).
[54]D. Zhang, Z. Nie, Z. Wang, L. Huang, Q. Zhang, and Y. Dong Wang, J. Magn. Magn. Mater. **387**, 107 (2015).
[55]T. Gao, M. Wu, N. Qi, T. Zhou, X. Luo, Y. Liu, K. Xu, V. V. Marchenkov, H. Dong, Z. Chen, and B. Chen, J. Alloys Compd. **753**, 149 (2018).
[56]J. B. A. Hamer, R. Daou, S. Özcan, N. D. Mathur, D. J. Fray, and K. G. Sandeman, J. Magn. Magn. Mater. **321**, 3535 (2009).
[57]Y. K. Fang, C. C. Yeh, C. W. Chang, W. C. Chang, M. G. Zhu, and W. Li, Scr. Mater. **57**, 453 (2007).
[58]J. Liu, K. Skokov, and O. Gutfleisch, Scr. Mater. **66**, 642 (2012).
[59]Y. Song, S. Chen, S. Ma, Z. Zhang, K. Liu, S. U. Rehman, K. Yang, H. Zeng, Y. Zhang, C. Chen, X. Luo, and Z. Zhong, J. Magn. Magn. Mater. **495**, 165865 (2020).
[60]N. T. Trung, L. Zhang, L. Caron, K. H. J. Buschow, and E. Brück, Appl. Phys. Lett. **96**, 172504 (2010).
[61]J.-T. Wang, D.-S. Wang, C. Chen, O. Nashima, T. Kanomata, H. Mizuseki, and Y. Kawazoe, Appl. Phys. Lett. **89**, 262504 (2006).
[62]E. K. Liu, W. Zhu, L. Feng, J. L. Chen, W. H. Wang, G. H. Wu, H. Y. Liu, F. B. Meng, H. Z. Luo, and Y. X. Li, Europhys. Lett. **91**, 17003 (2010).
[63]T. Kanomata, H. Ishigaki, T. Suzuki, H. Yoshida, S. Abe, and T. Kaneko, J. Magn. Magn. Mater. **140-144**, 131 (1995).
[64]K. Noguchi, R. Kobayashi, Y. Mitsui, R. Y. Umetsu, J. Gouchi, Y. Uwatoko, and K. Koyama, J. Magn. Magn. Mater. **499**, 166199 (2020).
[65]Y. Li, Q. Zeng, Z. Wei, E. Liu, X. Han, Z. Du, L. Li, X. Xi, W. Wang, S. Wang, and G. Wu, Acta Mater. **174**, 289 (2019).
[66]C. F. Sánchez-Valdés, J. L. S. Llamazares, H. F.-Z. Niga, D. Ríos-Jara, P. Alvarez-Alonso, and P. Gorria, Scr. Mater. **69**, 211 (2013).
[67]S. Nizioł, A. Zięba, R. Zach, M. Baj, and L. Dmowski, J. Magn. Magn. Mater. **38**, 205 (1983).
[68]M. A. Wheeler, Phys. Rev. **41**, 331 (1932).
[69]K. A. Gschneidner and V. K. Pecharsky, Annu. Rev. Mater. Sci. **30**, 387 (2000).
[70]L. D. Griffith, Y. Mudryk, J. Slaughter, and V. K. Pecharsky, J. Appl. Phys. **123**, 034902 (2018).
[71]T. Samanta, D. L. Lepkowski, A. Us Saleheen, A. Shankar, J. Prestigiacomo, I. Dubenko, A. Quetz, I. W. H. Oswald, G. T. McCandless, J. Y. Chan, P. W. Adams, D. P. Young, N. Ali, and S. Stadler, J. Appl. Phys. **117**, 123911 (2015).
[72]T. Samanta, D. L. Lepkowski, A. Us Saleheen, A. Shankar, J. Prestigiacomo, I. Dubenko, A. Quetz, I. W. H. Oswald, G. T. McCandless, J. Y. Chan, P. W. Adams, D. P. Young, N. Ali, and S. Stadler, Phys. Rev. B **91**, 020401(R) (2015).
[73]A. C. Larson and R. B. Von Dreele, "General structure analysis system (GSAS)," Report LAUR 86-748 (Los Alamos National Laboratory, 2004).
[74]B. H. Toby, J. Appl. Cryst. **34**, 210 (2001).
[75]C. Hammond, *The Basics of Crystallography and Diffraction*, 3rd ed., International Union of Crystallography Texts on Crystallography (Oxford University Press, 2009), p. 243.
[76]V. K. Pecharsky and P. Y. Zavalij, *Fundamentals of Powder Diffraction and Structural Characterization of Materials*, 2nd ed. (Springer Science+Business Media, 2009), p. 640.
[77]J.-H. Chen, A. Us Saleheen, S. K. Karna, D. P. Young, I. Dubenko, N. Ali, and S. Stadler, J. Appl. Phys. **124**, 203903 (2018).
[78]J.-H. Chen, T. Poudel Chhetri, A. Us Saleheen, D. P. Young, I. Dubenko, N. Ali, and S. Stadler, Intermetallics **112**, 106547 (2019).
[79]Y.-Y. Zhao, F.-X. Hu, L.-F. Bao, J. Wang, H. Wu, Q.-Z. Huang, R.-R. Wu, Y. Liu, F.-R. Shen, H. Kuang, M. Zhang, W.-L. Zuo, X.-Q. Zheng, J.-R. Sun, and B.-G. Shen, J. Am. Chem. Soc. **137**, 1746 (2015).
[80]M. Mito and M. Hamada, "Piston cylinder-type high-pressure generating device," U.S. patent 8,789,456 B2 (29 July 2014).
[81]M. Mito, J. Phys. Soc. Jpn. **76**, 182 (2007).
[82]A. H. Morrish, *The Physical Principles of Magnetism* (John Wiley & Sons, Inc., 2001), Chap. 7.
[83]B. D. Cullity and C. D. Graham, *Introduction to Magnetic Materials* (John Wiley & Sons, Inc., 2011), Chap. 9.
[84]T. Kanomata, H. Ishigaki, K. Sato, M. Sato, T. Shinohara, F. Wagatsuma, and T. Kaneko, J. Magn. Soc. Jpn. **23**, 418 (1999).
[85]S. Kaprzyk and S. Nizioł, J. Magn. Magn. Mater. **87**, 267 (1990).
[86]S. Nizioł, R. Fruchart, and J. Senateur, J. Magn. Magn. Mater. **15–18**, 481 (1980).
[87]A. Szytuła, A. T. Pędziwiatr, Z. Tomkowicz, and W. Bażela, J. Magn. Magn. Mater. **25**, 176 (1981).
[88]C. Kittel, *Introduction to Solid State Physics*, 7th ed. (John Wiley & Sons, Inc., 2007), Chap. 15.
[89]J. S. Amaral and V. S. Amaral, J. Magn. Magn. Mater. **322**, 1552 (2010).
[90]J.-H. Chen, A. Us Saleheen, P. W. Adams, D. P. Young, N. Ali, and S. Stadler, J. Appl. Phys. **123**, 145101 (2018).
[91]L. Caron, Z. Q. Ou, T. T. Nguyen, D. T. C. Thanh, O. Tegus, and E. Brück, J. Magn. Magn. Mater. **321**, 3559 (2009).